

1 **Determination of the parameters affecting electrospun chitosan fiber**
2 **size distribution and morphology**

3

4 V. Sencadas¹; D. M. Correia²; A. Areias¹; G. Botelho²; A. M. Fonseca²; I. C. Neves²; J.
5 L. Gómez-Ribelles^{3,4,5} and S. Lanceros-Mendez¹

6

7 ¹ *Centro/Departamento de Física, Universidade do Minho, Campus de Gualtar, 4710-*
8 *058 Braga, Portugal*

9 ² *Dept. Química, Centro de Química, Universidade do Minho, Campus de Gualtar,*
10 *4710-057 Braga, Portugal;*

11 ³ *Centro de Biomateriales e Ingeniería Tisular, Universidad Politécnica de Valencia,*
12 *Camino de Ver s/n, 46022 Valencia, Spain*

13 ⁴ *Centro de Investigación Príncipe Felipe, Autopista del Saler 16, 46013 Valencia,*
14 *Spain*

15 ⁵ *CIBER en Bioingeniería, Biomateriales y Nanomedicina, Valencia, Spain*

16 *e-mail: vsencadas@fisica.uminho.pt

17

18 **Abstract**

19 The production of chitosan nanofiber mats by electrospinning presents serious
20 difficulties due to the lack of suitable solvents and the strong influence of processing

21 parameters on the fiber properties. Two are the main problems to be solved: to control
22 the properties of the solution in order to obtain large area uniform fiber mats by having
23 a stable flow rate and to avoid sparks during the process, damaging the fiber mats. In
24 this work chitosan electrospun mats have been prepared from solutions of
25 trifluoroacetic acid / dichloromethane mixtures, allowing to solve the aforementioned
26 problems. Mats with uniform fibers of submicron diameters without beads were
27 obtained. Further, the influence of the different solution and process parameters on the
28 mean fiber diameter and on the width of the distribution of the fiber sizes has been
29 assessed. Solvent composition, needle diameter, applied voltage and traveling distance
30 were the parameters considered in this study.

31

32 **Introduction**

33 Increasing attention has been given in recent years to natural polymers, such as
34 polysaccharides, due to their abundance in nature, unique structures and characteristics
35 with respect to synthetic polymers (Honarkar & Barikani, 2009). Chitosan is a natural
36 linear polysaccharide composed of glucosamine and N-acetyl glucosamine units linked
37 by β (1-4) glycosidic bonds. Although naturally present in some microorganisms and
38 fungi, commercial chitosan is industrially produced by partial deacetylation of chitin by
39 removal of acetamide groups. Chitin is the second most abundant natural
40 polysaccharide after cellulose. It is mainly found in crustacean shells (shrimp, crab,
41 etc.), insect cuticle and cell walls of fungi (Baldrick, 2010; Fernandez-Megia, Novoa-
42 Carballal, Quiñoá & Riguera, 2005; Krajewska, 2005; Malafaya, Silva & Reis, 2007;
43 Ravi Kumar, 2000). The degree of deacetylation, DD, which defines the distinction
44 between chitin and chitosan, is not precisely established.

45 The term chitosan is found in the literature to describe polymers of chitosan with
46 different molecular weights, viscosity and degree of deacetylation (40-98 %) (Baldrick,
47 2010). However, the term chitosan is generally applied when the degree of deacetylation
48 is above 70 % and the term chitin is used when the degree of deacetylation is below
49 20% (Baldrick, 2010).

50 Chitosan in its crystalline form is usually insoluble in aqueous solutions above a pH of
51 ~7. However, due to the existence of primary amine groups, the structure can be
52 protonated and the protonate free amine groups on glucosamine facilitate the solubility
53 of the molecule, being therefore highly soluble in acid pH (Pillai, Paul & Sharma, 2009;
54 Yaghobi & Hormozi, 2010).

55 Chitosan offers many structural possibilities for chemical modifications in order to
56 induce novel properties, functions and applications, in particular in the biomedical area.
57 It is nontoxic, biocompatible and biodegradable and therefore an excellent material for
58 biomedical applications (Jayakumar, Menon, Manzoor, Nair & Tamura, 2010;
59 Jayakumar, Prabakaran, Nair, Tokura, Tamura & Selvamurugan, 2010; Jayakumar,
60 Prabakaran, Sudheesh Kumar, Nair & Tamura, 2011).

61 Recently, much attention has been paid to chitosan based nanofibers as biomaterial.
62 There are several methods for the fabrication of nanofibers, making use of chemical,
63 thermal and electrostatic principles (Beachley & Wen, 2010). The polymer nanofiber
64 fabrication methods most commonly associated with biomedical applications are
65 electrospinning, self-assembling, peptide reactions and phase separation. The
66 electrospinning process has attracted much attention for the production of polymer
67 fibers as it can produce them with diameters in the range from several micrometers
68 down to tens of nanometers, depending on the polymer and processing conditions
69 (Jayakumar, Prabakaran, Nair & Tamura). The nanofibers produced by this technique

70 are formed from a liquid polymer solution or melt that is feed through a capillary tube
71 into a region of an electric field generated by connecting a high voltage power source to
72 the capillary tube.

73 Chitosan nanofibers were successfully prepared by Ohkawa et al. (Ohkawa, Cha, Kim,
74 Nishida & Yamamoto, 2004). The authors studied the solvent effect on the morphology
75 of electrospun chitosan nanofibers by varying chitosan relative concentration with
76 different solvents. The solvents tested were diluted hydrochloric acid, acetic acid,
77 formic acid and trifluoroacetic acid (TFA). It was found that when the concentration of
78 chitosan increased, the morphology of the deposited fibers on the collector changed
79 from spherical beads to an interconnected fibrous system. Further, the addition of
80 dichloromethane (DCM) to the chitosan/TFA solution improved the homogeneity of the
81 electrospun chitosan nanofibers. Electrospinning conditions were optimized in order to
82 obtain homogeneous chitosan nanofibers with an average diameter of 330 nm. Other
83 studies on electrospun chitosan nanofibers have been also reported (Jayakumar,
84 Prabakaran, Nair & Tamura). Schiffman et al. obtained bead-free electrospun chitosan
85 nanofibers from a solution of TFA and chitosan with different molecular weights. A
86 small correlation between viscosity and fiber diameter was found (Schiffman &
87 Schauer, 2006, 2007). Despite these efforts, large fiber mats with controlled fiber
88 dimensions are not obtained mainly due to the large electrical conductivity of the TFA
89 solvent, which leads to an unstable process in which the flow rate is controlled by the
90 electric field more than by the dispenser. Further, electrical sparks often occur,
91 damaging parts of the samples. In fact, almost no cell cultures have been reported until
92 now in pure chitosan electrospun fiber mats (Jayakumar, Prabakaran, Nair, Tokura,
93 Tamura & Selvamurugan, 2010; Jayakumar, Prabakaran, Sudheesh Kumar, Nair &
94 Tamura, 2011).

95 The electrospinning technique is very versatile and a wide range of parameters can play
96 an important role in obtaining the desired nanofiber size and microstructure. These
97 parameters include solution viscosity, voltage, feed rate, solution conductivity,
98 capillary-to-collector distance and capillary tube size (Bhardwaj & Kundu; Sill & von
99 Recum, 2008). In this work, a systematic study has been performed in order to solve the
100 aforementioned main problems. By controlling solution parameters a stable process has
101 been achieved allowing obtaining large fiber mats with tailored fiber dimension.
102 Further, the effect of the main processing parameters such as solvent concentration,
103 flow rate, applied voltage, feed rate and inner needle diameter on the chitosan fiber
104 characteristics and sample morphology has been studied in order to set the ground for a
105 systematic and reproducible way to obtain chitosan nanofiber samples for specific
106 applications.

107

108 **Experimental**

109 *Materials*

110 Chitosan practical grade polymer was purchased from Sigma-Aldrich with ≥ 75 %
111 degree of D-acetylation. Dichloromethane (DCM) and Trifluoroacetic acid (TFA, 99 %
112 ReagentPlus) were purchased from Sigma-Aldrich (Table 1). All materials were used as
113 received from the provider.

114

115 **Table 1** – (Budavari, 1996).

116

117

118

119 *Preparation of the solution*

120

121 The polymer was dissolved in a TFA/DCM solution with different TFA/DCM volume
122 ratios for a 7 % (weight) of chitosan. The solution were prepared under a constant and
123 vigorous magnetic stirring (JPSelecta, Agimatic-E) at room temperature until complete
124 dissolution of the chitosan. The viscosity of the prepared solutions was measured in a
125 Viscostar Plus set-up from Fungilab. The variation of the viscosity of the polymer
126 solution with varying TFA/DCM ratio is represented in figure 1.

127

128

129 *Electrospinning*

130 The polymer solution was placed in a commercial plastic syringe fitted with a steel
131 needle. The inner diameter of the needle was 0.5, 1.0 and 1.7 mm for different
132 experiments. Electrospinning was conducted by applying a voltage ranging from 20 and
133 30 kV with a PS/FC30P04 power source from Glassman. A syringe pump
134 (Syringepump) fed the polymer solution into the tip at a rate between 1 and 8 ml.h⁻¹.
135 The electrospun samples were collected on a grounded collecting plate placed at
136 different distances from 50 to 200 mm from the needle tip.

137

138 *Characterization*

139 Electrospun fibers were coated with a thin gold layer using a sputter coater from
140 Polaron (SC502) and the morphology of the membranes were observed by scanning
141 electron microscopy (SEM, JSM-6300 from JEOL) at an accelerating voltage of 15 kV.
142 The fiber diameter distribution was calculated over 50 fibers with the Image J software
143 (J, 2011) from the SEM images obtained at a magnification of 3500 x.

144 The degree of deacetylation was determined by nuclear magnetic resonance (NMR)
145 according to the procedure described in (Fernandez-Megia, Novoa-Carballal, Quiñoá &
146 Riguera, 2005). Five milligram of chitosan after and before electrospun were added to a
147 5 mm NMR tube containing 0.5 mL of 2 % deuterium chloride (DCI, from Fluka)
148 solution in deuterated water (D₂O, Mw=20,02, ACROS Organics) and heated at 70 °C
149 for 1 h in order to speed up the dissolution. The results for the ¹NMR were collected in a
150 Varian Unity Plus 300 at 70 °C.

151

152

153 **Results and Discussion**

154

155 Several parameters affect the fiber morphology and size distribution of the polymer
156 electrospun fibers. Among the most important ones are those corresponding to the initial
157 polymer solution: parameters related to the solvent used (dielectric constant, volatility,
158 boiling point and others), the solution concentration (that controls the viscosity) and the
159 molecular weight of the polymer (that allows polymer entanglement). The main
160 parameters that control the jet formation and solvent evaporation rate are the feed rate
161 through the needle and needle diameter, traveling distance from the needle to the
162 collector, temperature and electric field (Ribeiro, Sencadas, Ribelles & Lanceros-
163 Méndez, 2010; S. Ramakrishna, K. Fujihara, W. E. Teo, T. C. Lim & Ma, 2005; Teo &
164 Ramakrishna, 2006).

165 TFA is a strong acid that can dissolve the polymer through the formation of salts that
166 destroy the strong interactions that exist between the molecules of chitosan (Ohkawa,
167 Cha, Kim, Nishida & Yamamoto, 2004). The salt formation occurs between the TFA
168 and the amino groups along the chitosan chain after the following sequential steps: first,

169 protonation of amine groups (-NH₂) along the chain of chitosan; second, ionic
170 interaction between protonated amino groups (-NH₃) and then formation of
171 trifluoroacetate anions. In this configuration, the salts are soluble in an aqueous media.
172 In this work, solutions of chitosan in TFA/DCM with different relative concentrations
173 were used in order to tailor viscosity and conductivity of the solvent. These parameters
174 have strong influence in the electrospinning process and therefore in the final fiber
175 morphology. The SEM images for the electrospun samples obtained from a solution of
176 chitosan with different TFA/DCM volume ratios and fixed traveling distance of 150
177 mm, needle diameter of 0.5 mm, flow rate of 2 ml.h⁻¹ and a voltage of 25 kV are
178 presented in Figure 2.

179 Schiffman et al. reported that electrospinning of chitosan in pure TFA solvent was viable
180 for lower chitosan concentrations (2.7 % (w/v)) (Schiffman & Schauer, 2006). In the
181 present work, it was difficult to stabilize the electrospinning process for TFA/DCM
182 concentrations rich in TFA solvent (higher than 80 % TFA) in the solution due to the
183 presence of sparks that frequently appeared during the fiber processing, even for small
184 applied electric fields, therefore hindering the electrospinning process. An increase of
185 TFA in the solution increases the viscosity (figure 1) and the conductivity of the
186 medium, which are at the origin of the sparks. Electrospinning involves stretching of the
187 solution caused by the repulsion of the charges at its surface. If the conductivity of the
188 solution is increased, more charges can be carried out by the electrospinning jet. The
189 free amines trifluoroacetate anions formed during the chitosan dissolution in TFA
190 increase the conductivity of the solution (Dannhauser & Cole, 1952) and, therefore, the
191 critical voltage for electrospinning to occur is reduced.

192 Further, for TFA/DCM solvent mixtures with low TFA content, the dissolution of the
193 polymer was extremely difficult and during the electrospinning process some drops

194 failed from the needle due to the lower viscosity of the solution, These drops completely
195 dissolved the formed fiber and destroyed the homogeneity of the electrospun mats. It
196 was also observed that the average fiber diameter of the electrospun mats decreased
197 with increasing DCM content in the solvent mixture. On the other hand, a larger fiber
198 size distribution was observed with increasing TFA content in the solution a (Figure 3).
199 Figure 3 was obtained from histograms analogous to those shown in Figure 2 (the ones
200 corresponding to Figures 2c and 2d are included in Figure 3), from which the mean
201 value was calculated. The bars in Figure 3 indicate the average and the standard
202 deviation of the fiber diameters.

203 The influence of the inner diameter of the needle in the average size of the electrospun
204 fibers was characterized. For the samples processed with a needle with an inner
205 diameter of 0.5 mm, the presence of very thin fibers with diameters ~ 250 nm was
206 observed. This fact can be attributed to the lower DCM solvent evaporation temperature
207 (Figure 4). On the other hand, the samples obtained with a higher needle diameter show
208 a more uniform fiber size distribution. It was also noted that all samples were free of
209 beads, indicating that the tested chitosan electrospinning conditions provide sufficient
210 chain entanglement for fiber formation.

211 The presence of small particles (Figure 4b) on the surface of the electrospun fibers has
212 been explained by Zhang et al. as a consequence of the presence of salts (Zhang, Yuan,
213 Wu, Han & Sheng, 2005) originated by the chitosan dissolution in the TFA acid, as
214 explained above. These salts are commonly observed for higher polymer concentrations
215 and higher TFA content in the chitosan-TFA/DCM solvent solution.

216 The average size of the fibers for the different needle inner diameters was calculated
217 and the results show a slight increase of the average fiber diameter from ~ 360 to 410
218 nm with increasing inner needle diameter (figure 5).

219 The fiber diameter distribution along the sample is quite similar for all the electrospun
220 samples, being therefore independent of the needle inner diameter. Literature shows
221 contradictory results in this point. Macossay et al. found no influence of the needle
222 diameter on the average fiber diameter of poly(methyl methacrylate) electrospun fibers
223 (Macossay, Marruffo, Rincon, Eubanks & Kuang, 2007), while Katti et al. and Ribeiro
224 et al. reported that the fiber diameter decreases with decreasing needle inner diameter
225 (Katti, Robinson, Ko & Laurencin, 2004; Ribeiro, Sencadas, Ribelles & Lanceros-
226 Méndez, 2010).

227 A decrease of the inner diameter of the needle causes a reduction of the droplet at the tip
228 and therefore the surface tension of the droplet increases. Then, for a given applied
229 voltage, a larger Coulombic force is required to cause the jet initiation, which results in
230 a decrease of the jet acceleration and, as a consequence, more time is required for the
231 solution to be stretched and elongated before it is collected (S. Ramakrishna, K.
232 Fujihara, W. E. Teo, T. C. Lim & Ma, 2005).

233 The influence of the distance between the needle tip to the grounded collector on the
234 fiber average diameter and distribution was also analyzed. It was observed that the
235 fibers with the smallest average diameter, ~260 nm, were obtained for the samples with
236 a 50 mm distance between needle tip and collector and that the mean fiber diameter
237 increases by increasing the distance between the needle tip and the collector. A
238 maximum average fiber diameter of ~ 500 nm was obtained for a traveling distance of
239 200 mm (Figure 6).

240 It was also observed that the mean diameter fiber distribution increases with increasing
241 the distance between needle tip and sample collector. The presence of sub-structures of
242 smaller fibers between the smooth large fibers (Figure 7) suggests the formation of a
243 secondary jet during the main electrospinning process due to the high solution viscosity

244 (Figure 1). Ding et al. (Ding & et al., 2006) pointed out that this fact is related to certain
245 processing conditions such as high voltage, low relative humidity and fast phase
246 separation of polymer and solvent during the flight between the needle and the collector.
247 Ramakrishna et al. (S. Ramakrishna, K. Fujihara, W. E. Teo, T. C. Lim & Ma, 2005)
248 justified these structures as a consequence of the formations and ejection of smaller jets
249 from the surface of the primary jets, which is comparable to the ejection of the initial jet
250 from the surface of a charged droplet. It was proposed that the elongation of the jet and
251 evaporation of the solvent modifies the shape and the charge density of the jet during
252 the traveling between the tip and the collector. Thus, the balance between the electrical
253 forces and surface tension can change, giving rise to instabilities in the shape of the jet.
254 Such instabilities can decrease the local charge per unit surface area by ejecting a
255 smaller jet from the surface of the primary jet or by splitting apart into two smaller jets.
256 In this work a blend of two solvents with different boiling points (Table 1) has been
257 used and the observed sub-structures of smaller fibers can be related to the fast
258 evaporation of the DCM solvent from the blend during the traveling from the needle tip
259 to the collector, leaving behind solidified fibers with smaller diameters than the ones
260 that crystallize later when the TFA solvent evaporates. This phenomenon was also
261 observed in Figures 2 and 3, when the effect of TFA/DCM solvent ratio on fiber
262 diameter and mat morphology was presented.

263 It is pointed out that an increase of the distance between the tip and the collector often
264 results in a decrease of the fiber diameter (S. Ramakrishna, K. Fujihara, W. E. Teo, T.
265 C. Lim & Ma, 2005). However, in the present work it was observed that the diameter of
266 the fibers increases for increasing distance between the needle tip and the grounded
267 collector. This behavior is to be ascribed to the decrease of the electrostatic field

268 strength resulting in a decrease of the electrostatic force and therefore on the stretching
269 of the fibers.

270 Tip to collector distance has a direct influence on the jet flight time and electric field
271 strength: a decrease of the distance shortens flight and solvent evaporation times and
272 increases the electric field strength. A decrease in the tip-collector distance has a similar
273 effect as increasing the voltage (Figure 8).

274 The changes in the applied electric field have strong influence on the shape of the
275 droplet at the needle tip, its surface charge, dripping rate, velocity of the flowing fluid
276 and hence on the fiber structure and morphology. Similarly, the needle tip to collector
277 distance also determines the time available for fiber drying and the space available for fiber
278 splaying and whipping to take place.

279 The high voltage will induce the necessary charge distribution on the solution and
280 initiate the electrospinning process when the electrostatic force overcomes the surface
281 tension of the solution (S. Ramakrishna, K. Fujihara, W. E. Teo, T. C. Lim & Ma,
282 2005). For higher electric fields, the jet will accelerate and stretch due to the larger
283 Coulombic forces, which results in a reduction of the fiber average diameter and also
284 promotes faster solvent evaporation to yield drier fibers (S. Ramakrishna, K. Fujihara,
285 W. E. Teo, T. C. Lim & Ma, 2005).

286 Finally, the influence of the feed rate on the average fiber distribution was characterized
287 (Figure 9). A minimum value of solution volume suspended at the end of the needle
288 should be maintained in order to form a stable Taylor cone (Teo & Ramakrishna, 2006).

289 The feed rate determines the amount of solution available for the electrospinning process.
290 Typically, when the feed rate increases, a corresponding increase of the fiber diameter is
291 observed, as observed i.e. for poly(vinylidene fluoride) (Ribeiro, Sencadas, Ribelles &
292 Lanceros-Méndez, 2010) and for poly(L-lactide acid) (Clarisse & et al., 2011). In

293 chitosan such behavior was not found and the fiber diameter distribution is quite similar
294 for the different feed rates within the range studied in the present work (Figure 9).

295 It was expected that increasing feed rate will increase the volume of the solution drawn
296 from the needle tip, and consequently the jet would take a longer time to dry. The lower
297 boiling point of the solvents used in this work (Table 1) allows the fast evaporation
298 during the flight time. In this situation, full solvent evaporation has already occurred
299 when the fiber reaches the grounded collector and therefore the feed rate does not have
300 influence on the fiber diameter.

301 Most of the physical and chemical properties of this biopolymer strongly depend on the
302 degree of deacetylation (DD) (Lavertu et al., 2003). The DD can be calculated from the
303 ¹NMR spectra (figure 10) through:

304

$$DD(\%) = \frac{H_1 D}{H_1 D + \left(\frac{H_{ac}}{3}\right)} \times 100$$

305

306

307 where H₁D is the peak corresponding to the H₁ proton of the deacetylated monomer
308 (duplet at δ= 4.858 ppm) and H_{ac} is the peak of the three protons of the acetyl group
309 (singlet at δ= 1.988 ppm) (Lavertu et al., 2003). The obtained results show that the
310 commercial chitosan has a DD of 78 %, which is similar to the value given by the
311 producer and also similar to the values obtained for the electrospun fibers. It is therefore
312 concluded that the electrospinning process does not affect the degree of deacetylation of
313 the polymer.

314

315 **Conclusions**

316 Large chitosan mats with uniform fibers of submicron diameters without beads have
317 been prepared from trifluoroacetic acid / dichloromethane mixture solutions by a stable
318 electrospinning process. It was observed that an increase of the DCM present in the
319 solvent blend solution produces nanofibers with smaller diameters and narrower
320 diameter distribution. Inclusion of DCM within the TFA solutions modifies solution
321 viscosity and electrical characteristics, leading to a stable flow rate and avoiding spark
322 formation. The inner diameter of the needle and the feed rate does not have influence in
323 the chitosan electrospun fiber diameter. On the other hand, it was observed that a
324 decrease of the distance from the needle tip to the grounded collector gives origin to
325 nanofibers with smaller diameters. Finally, an increase of the applied voltage also
326 decreases the nanofibers diameter. The degree of deacetylation of the polymer is not
327 affected by the electrospinning process.

328

329

330 **Acknowledgements**

331 This work is funded by FEDER funds through the "Programa Operacional Factores de
332 Competitividade – COMPETE" and by national funds by FCT- Fundação para a Ciência
333 e a Tecnologia, project references NANO/NMed-SD/0156/2007. V.S. thanks the FCT
334 for the SFRH/BPD/63148/2009 grants. JLGR acknowledge the support of the Spanish
335 Ministry of Science and Innovation through project No. MAT2010-21611-C03-01
336 (including the FEDER financial support) and Programa Nacional de
337 Internacionalización de la I+D project EUI2008-00126. Funding for research in the field
338 of Regenerative Medicine through the collaboration agreement from the Conselleria de
339 Sanidad (Generalitat Valenciana), and the Instituto de Salud Carlos III (Ministry of
340 Science and Innovation) is also acknowledged.

341 Thanks are due to the National NMR Network that was purchased within the framework
342 of the National Program for Scientific Re-equipment, contract REDE/1517/RMN/2005
343 with funds from POCI 2010 (FEDER) and FCT. Also thank to the UPV Microscopy
344 Service for the use of their lab.

345

346 **References**

347 Baldrick, P. (2010). The safety of chitosan as a pharmaceutical excipient. *Regulatory*
348 *Toxicology and Pharmacology*, 56(3), 290-299.

349 Beachley, V., & Wen, X. (2010). Polymer nanofibrous structures: Fabrication,
350 biofunctionalization, and cell interactions. *Progress in Polymer Science*, 35(7), 868-
351 892.

352 Bhardwaj, N., & Kundu, S. C. Electrospinning: A fascinating fiber fabrication
353 technique. *Biotechnology Advances*, 28(3), 325-347.

354 Budavari, S. (1996). *An Encyclopedia of Chemicals, Drugs, and Biologicals*. New
355 Jersey: Merck & Co.

356 Clarisse, R., & et al. (2011). Tailoring the morphology and crystallinity of poly(L-
357 lactide acid) electrospun membranes. *Science and Technology of Advanced Materials*,
358 12(1), 015001.

359 Dannhauser, W., & Cole, R. H. (1952). On the Dielectric Constant of Trifluoroacetic
360 Acid1. *Journal of the American Chemical Society*, 74(23), 6105-6105.

361 Ding, B., & et al. (2006). Formation of novel 2D polymer nanowebs via
362 electrospinning. *Nanotechnology*, 17(15), 3685.

363 Fernandez-Megia, E., Novoa-Carballal, R., Quiñoá, E., & Riguera, R. (2005). Optimal
364 routine conditions for the determination of the degree of acetylation of chitosan by ¹H-
365 NMR. *Carbohydrate Polymers*, 61(2), 155-161.

366 Honarkar, H., & Barikani, M. (2009). Applications of biopolymers I: chitosan.
367 *Monatshefte Fur Chemie, 140*(12), 1403-1420.

368 J, I. (2011). Image Processing and Analysis in Java available from
369 <http://rsbweb.nih.gov/ij/index.html>.

370 Jayakumar, R., Menon, D., Manzoor, K., Nair, S. V., & Tamura, H. (2010). Biomedical
371 applications of chitin and chitosan based nanomaterials--A short review. *Carbohydrate*
372 *Polymers, 82*(2), 227-232.

373 Jayakumar, R., Prabakaran, M., Nair, S. V., & Tamura, H. Novel chitin and chitosan
374 nanofibers in biomedical applications. *Biotechnology Advances, 28*(1), 142-150.

375 Jayakumar, R., Prabakaran, M., Nair, S. V., Tokura, S., Tamura, H., & Selvamurugan,
376 N. (2010). Novel carboxymethyl derivatives of chitin and chitosan materials and their
377 biomedical applications. *Progress in Materials Science, 55*(7), 675-709.

378 Jayakumar, R., Prabakaran, M., Sudheesh Kumar, P. T., Nair, S. V., & Tamura, H.
379 (2011). Biomaterials based on chitin and chitosan in wound dressing applications.
380 *Biotechnology Advances, 29*(3), 322-337.

381 Katti, D. S., Robinson, K. W., Ko, F. K., & Laurencin, C. T. (2004). Bioresorbable
382 nanofiber-based systems for wound healing and drug delivery: Optimization of
383 fabrication parameters. *Journal of Biomedical Materials Research Part B: Applied*
384 *Biomaterials, 70B*(2), 286-296.

385 Krajewska, B. (2005). Membrane-based processes performed with use of chitin/chitosan
386 materials. *Separation and Purification Technology, 41*(3), 305-312.

387 Lavertu, M., Xia, Z., Serreghi, A. N., Berrada, M., Rodrigues, A., Wang, D., Buschmann,
388 M. D., & Gupta, A. (2003). A validated ¹H NMR method for the determination of the
389 degree of deacetylation of chitosan. *Journal of Pharmaceutical and Biomedical*
390 *Analysis, 32*(6), 1149-1158.

391 Macossay, J., Marruffo, A., Rincon, R., Eubanks, T., & Kuang, A. (2007). Effect of
392 needle diameter on nanofiber diameter and thermal properties of electrospun
393 poly(methyl methacrylate). *Polymers for Advanced Technologies*, 18(3), 180-183.

394 Malafaya, P. B., Silva, G. A., & Reis, R. L. (2007). Natural-origin polymers as carriers
395 and scaffolds for biomolecules and cell delivery in tissue engineering applications.
396 *Advanced Drug Delivery Reviews*, 59(4-5), 207-233.

397 Ohkawa, K., Cha, D., Kim, H., Nishida, A., & Yamamoto, H. (2004). Electrospinning
398 of Chitosan. *Macromolecular Rapid Communications*, 25(18), 1600-1605.

399 Pillai, C. K. S., Paul, W., & Sharma, C. P. (2009). Chitin and chitosan polymers:
400 Chemistry, solubility and fiber formation. *Progress in Polymer Science*, 34(7), 641-678.

401 Ravi Kumar, M. N. V. (2000). A review of chitin and chitosan applications. *Reactive*
402 *and Functional Polymers*, 46(1), 1-27.

403 Ribeiro, C., Sencadas, V., Ribelles, J. L. G., & Lanceros-Méndez, S. (2010). Influence
404 of Processing Conditions on Polymorphism and Nanofiber Morphology of Electroactive
405 Poly(vinylidene fluoride) Electrospun Membranes. *Soft Materials*, 8(3), 274 - 287.

406 S. Ramakrishna, K. Fujihara, W. E. Teo, T. C. Lim, & Ma, Z. (2005). *Introduction to*
407 *electrospinning and nanofibers*. Singapore: World Scientific.

408 Schiffman, J. D., & Schauer, C. L. (2006). Cross-Linking Chitosan Nanofibers.
409 *Biomacromolecules*, 8(2), 594-601.

410 Schiffman, J. D., & Schauer, C. L. (2007). One-Step Electrospinning of Cross-Linked
411 Chitosan Fibers. *Biomacromolecules*, 8(9), 2665-2667.

412 Sill, T. J., & von Recum, H. A. (2008). Electrospinning: Applications in drug delivery
413 and tissue engineering. *Biomaterials*, 29(13), 1989-2006.

414 Teo, W. E., & Ramakrishna, S. (2006). A review on electrospinning design and
415 nanofibre assemblies. *Nanotechnology*, 17(14), R89.

416 Yaghoobi, N., & Hormozi, F. (2010). Multistage deacetylation of chitin: Kinetics study.
417 *Carbohydrate Polymers*, 81(4), 892-896.

418 Zhang, C., Yuan, X., Wu, L., Han, Y., & Sheng, J. (2005). Study on morphology of
419 electrospun poly(vinyl alcohol) mats. *European Polymer Journal*, 41(3), 423-432.

420

421 **Figure 1** – Variation of the viscosity of the polymer solution with varying TFA/DCM
422 ratio. The line is just a guide for the eyes.

423

424 **Figure 2** – Morphology of the chitosan mats for the samples obtained with a 7 % (w/v)
425 polymer solution at a traveling distance of 150 mm, needle diameter of 0.5 mm, flow
426 rate of 2 ml.h⁻¹ and a voltage of 25 kV: a) 80:20 and b) 60:40 TFA/DCM (v/v) solution;
427 c) and d) represent the fiber diameter histograms of the corresponding figures.

428

429 **Figure 3** – Influence of the TFA/DCM volume ratio in the distribution of fiber
430 diameters in the electrospun mats obtained for a 7 % (w/v) chitosan solution at a fixed
431 traveling distance of 150 mm, needle diameter of 0.5 mm, flow rate of 2 ml.h⁻¹ and a
432 voltage of 25 kV.

433

434 **Figure 4** – Morphology of the chitosan mats for the samples obtained for a 7 % (w/v)
435 polymer solution, a 70/30 TFA/DCM solvent solution, a traveling distance of 150 mm,
436 flow rate of 2 ml.h⁻¹ and a voltage of 25 kV for needle inner diameters of a) 0.5 mm and
437 b) 1.7 mm; c) and d) represent the fiber diameter histograms of the corresponding
438 figures.

439

440

441 **Figure 5** – Influence of the inner diameter of the needle in the average fiber diameter
442 and distribution for the electrospun mats obtained for a 7 % (w/v) chitosan solution, a
443 70/30 TFA/DCM solvent solution, a traveling distance of 150 mm, flow rate of 2 ml.h⁻¹
444 and a voltage of 25 kV.

445

446

447 **Figure 6** – Influence of the traveling distance on the fiber average diameter and
448 distribution in the electrospun mats obtained for a 7 % (w/v) chitosan solution, a 70/30
449 TFA/DCM solvent solution, a needle inner diameter of 0.5 mm, a flow rate of 2 ml.h⁻¹
450 and a voltage of 25 kV.

451

452

453 **Figure 7** – Morphology of the chitosan mats for the samples obtained for a 7 % (w/v)
454 polymer solution, a 70/30 TFA/DCM solvent solution and a needle diameter of 0.5 mm,
455 at a traveling distance of 150 mm, flow rate of 2 ml.h⁻¹ a voltage of 25 kV and a
456 distance between the needle tip to the sample collector of a) 50 mm and b) 200 mm.

457

458

459 **Figure 8** – Influence of the applied voltage on fiber average diameter and distribution in
460 the electrospun mats obtained for a 7 % (w/v) chitosan solution, a 70/30 TFA/DCM
461 solvent solution, needle inner diameter of 1.7 mm, flow rate of 2 ml.h⁻¹ and a traveling
462 distance of 15 cm.

463

464 **Figure 9** – Influence of the feed rate on the average fiber diameter and distribution of
465 the electrospun mats obtained for a 7 % (w/v) chitosan solution, a 70/30 TFA/DCM
466 solvent solution, needle inner diameter of 0.5 mm, flow rate of 2 ml.h⁻¹, a traveling
467 distance of 15 cm and a 25 kV applied voltage.

468

469 **Figure 10** – ¹H-NMR spectra of electrospun chitosan nanofibers at 70 °C.

470

471 **Table 1** – Properties of the solvents used in the present work [17].

472

473

474

475 Table 1

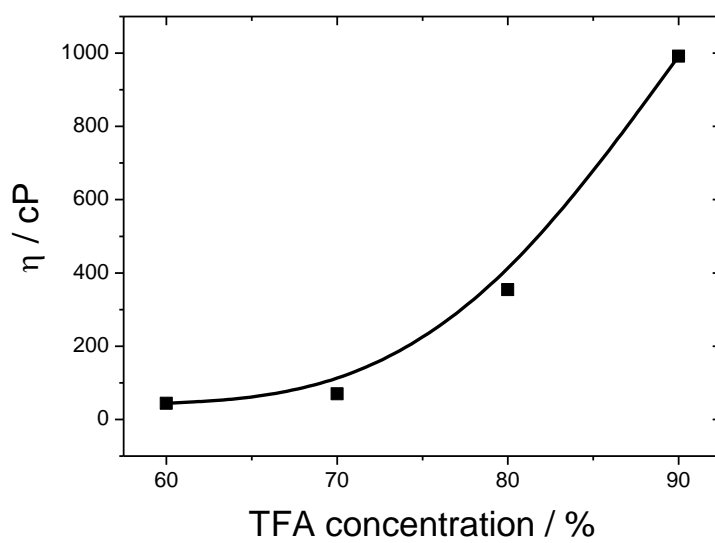
Solvent	Melting Point	Boiling Point	Density	Dipole Moment	Dielectric Constant
	°C	°C	g.cm ⁻³	Debye	
TFA	-15.2	73.0	1.535	2.28	8.42
DCM	-95.1	40.0	1.327	1.60	8.93

476

477

478

479 Figure 1

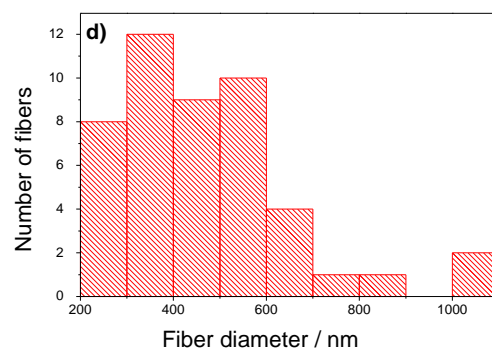
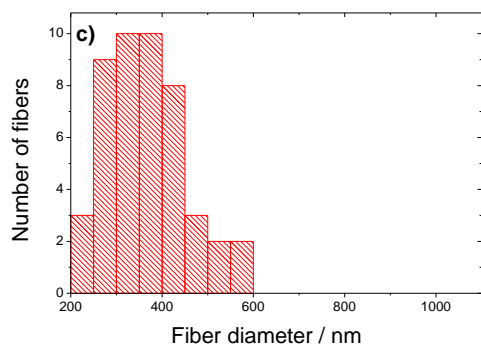
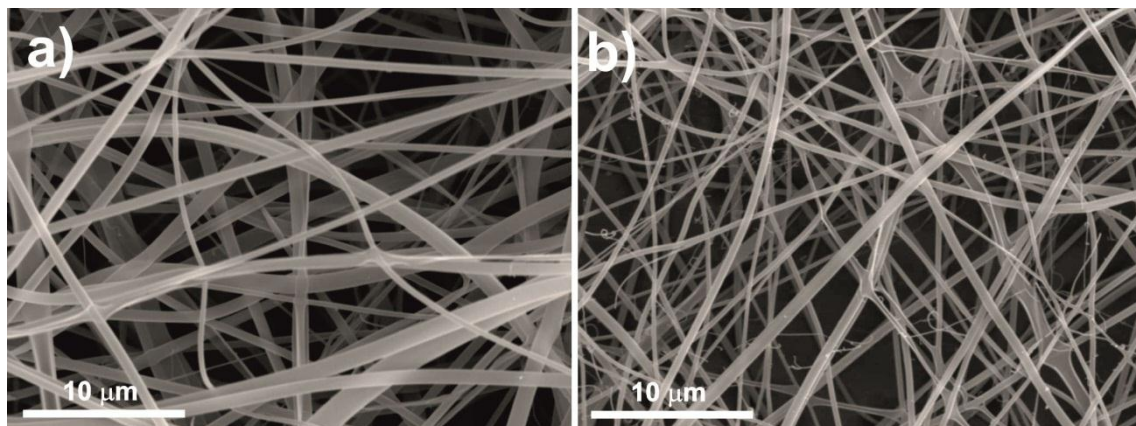


480

481

482 Figure 2

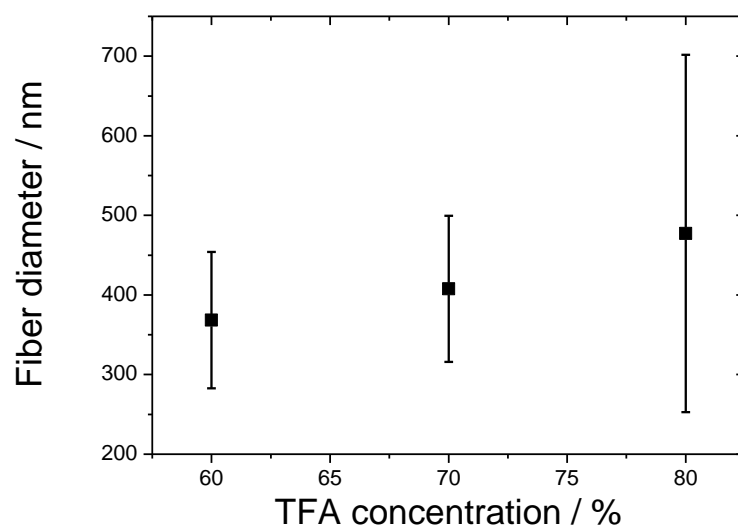
483



484

485

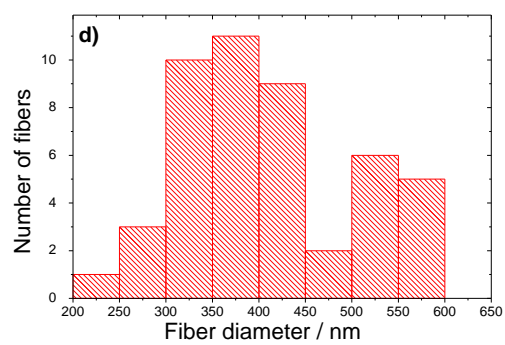
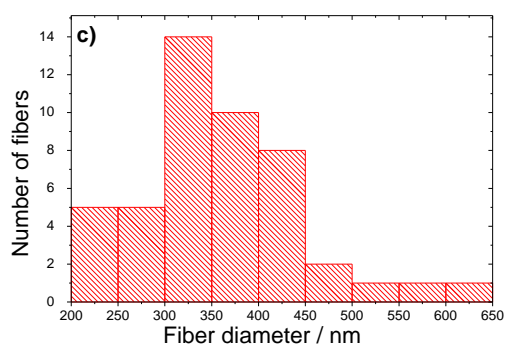
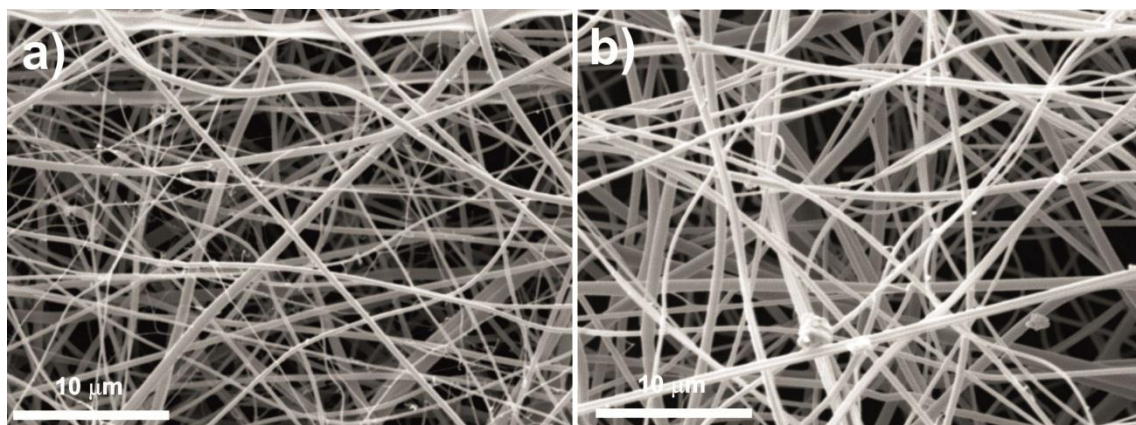
486 Figure 3



487

488

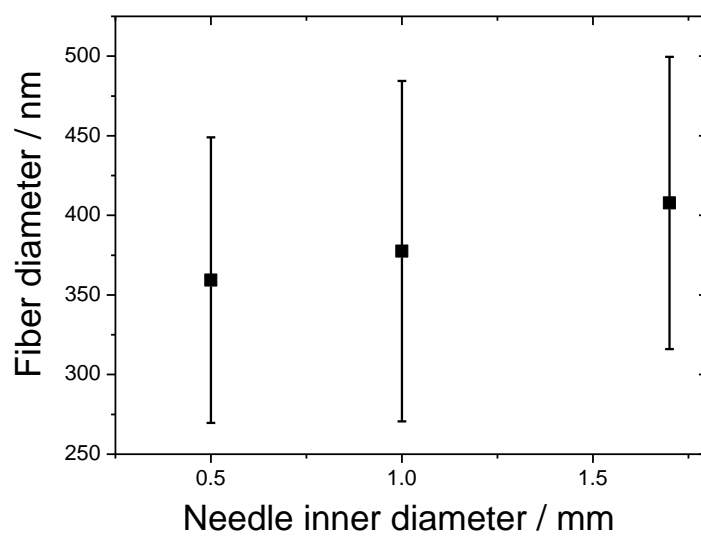
489 Figure 4



490

491

492 Figure 5

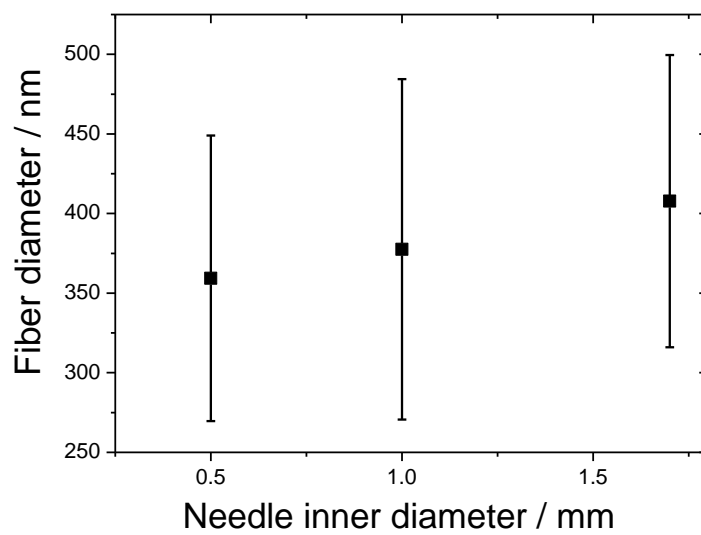


493

494

495 Figure 6

496

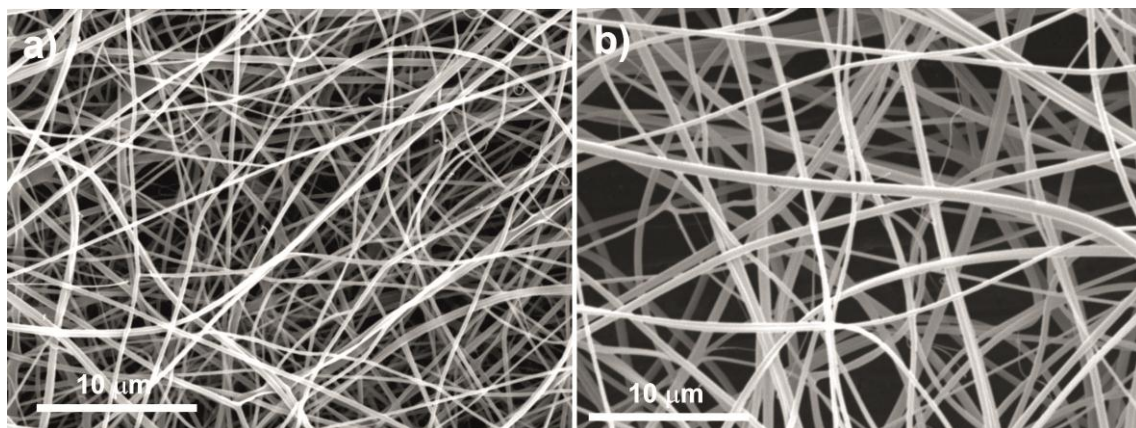


497

498

499 Figure 7

500

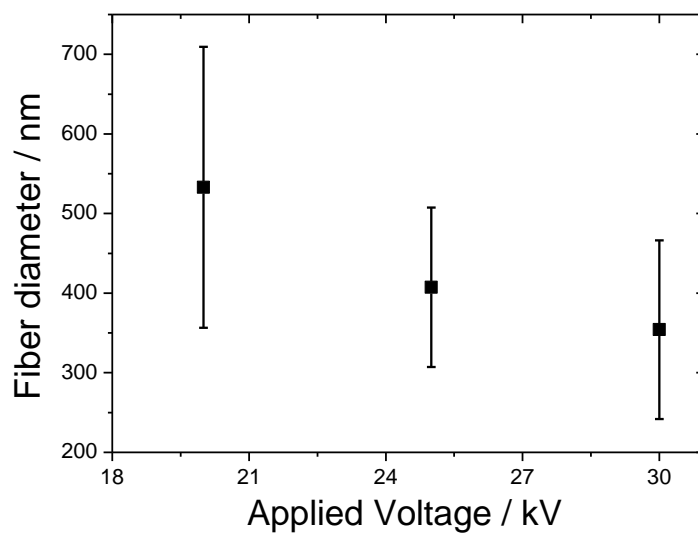


501

502

503 Figure 8

504

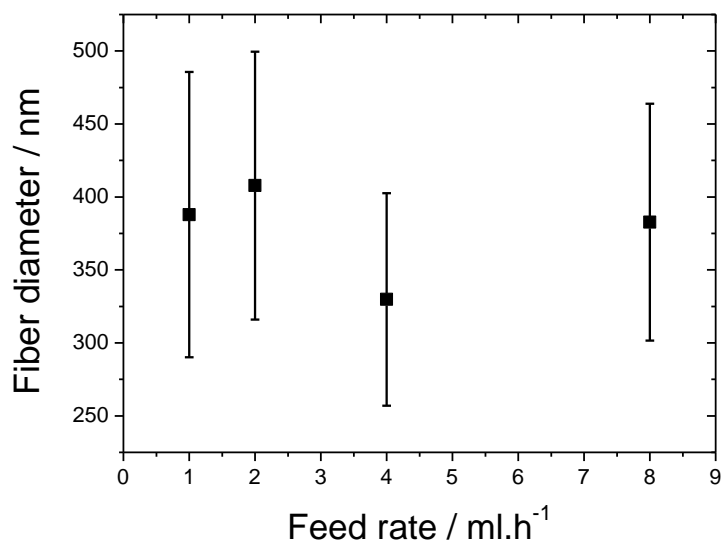


505

506

507 Figure 9

508

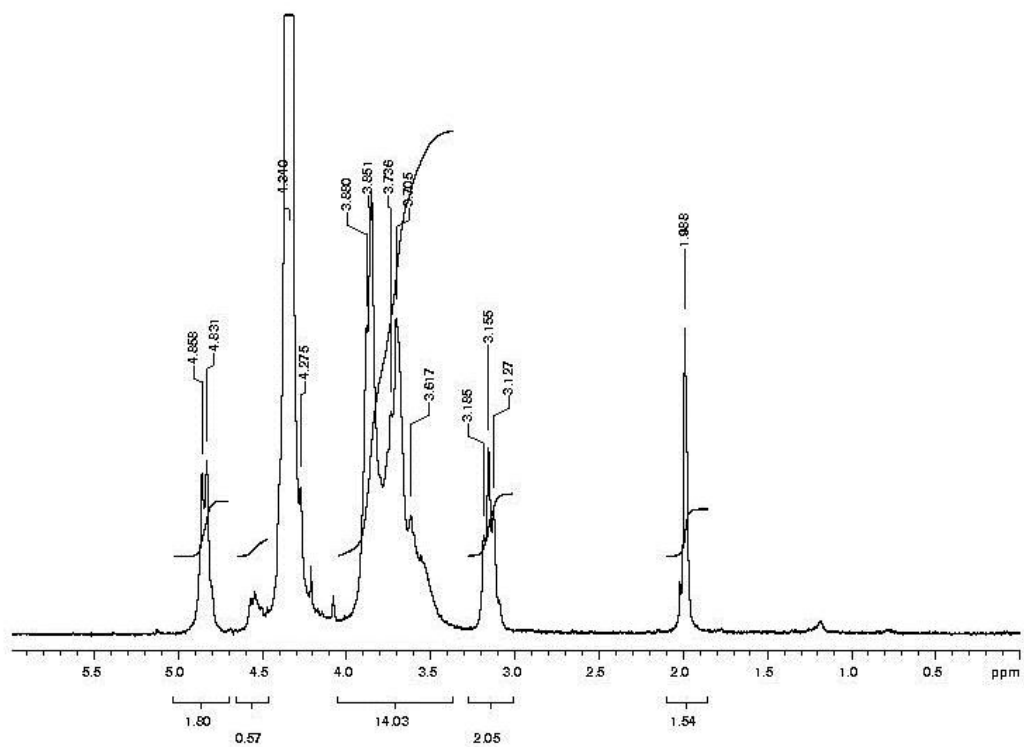


509

510

511 Figure 10

512



513

514